Peak Cancellation Signal-Based Parallel PAPR Reduction Method Using Low-Dimensional Null Space in Massive MIMO-OFDM

Jun Saito*, Takanori Hara†, and Kenichi Higuchi‡
*†‡Graduate School of Science and Technology, Tokyo University of Science
E-mail: *7322547@ed.tus.ac.jp, †t.hara@ieee.org, ‡higuchik@rs.tus.ac.jp

Abstract—**We investigate the peak-to-average power ratio (PAPR) reduction method in downlink massive multi-user multiple-input multiple-output (MIMO)-orthogonal frequency division multiplexing (OFDM) transmission. In this paper, we develop a new complexity-reduced PAPR reduction method based on peak cancellation (PC) signals using the null space in a MIMO channel for MIMO-OFDM signals. The proposed method divides the transmitter antennas jointly considered in the PAPR reduction process and utilizes the low-dimensional null space in the MIMO channel to reduce the computational complexity in the PAPR reduction process. Besides, it can execute PAPR reduction based on PC signals in parallel, suppressing the degradation of PAPR reduction capability due to the reduction of the dimension of the null space in the MIMO channel. Computer simulation results show that the proposed method significantly reduces computational complexity while keeping a sufficient PAPR reduction capability.**

I. INTRODUCTION

In future wireless communications systems such as 6G, an extremely high data rate will be demanded. As one of the promising technologies, terahertz (THz) communications have been much gained attention since wide bandwidth is available. Meanwhile, the signal in THz communications suffers from very high path loss [1]. Hence, downlink orthogonal frequency division multiplexing (OFDM)-based multi-user (MU) massive multiple-input multiple-output (MIMO) [2, 3] transmission with beamforming (BF) is essential to extend the range of mobile broadband. However, peak-to-average power ratio (PAPR) of the OFDM signals is usually very high, which is further enhanced because of the difference in the levels of transmission power among the transmitter antennas caused by the BF process in massive MIMO. In a massive MIMO environment, the cost and size of power amplifier for each transmission antenna are desired to be low. Therefore, the PAPR reduction is essential to realize massive MIMO-OFDM transmission with BF.

In a massive MU-MIMO downlink scenario, to reduce PAPR, a large number of methods that do not require any processing at each receiver (user terminal) side have been actively investigated. They utilize various techniques, such as tone reservation [4], antenna reservation [5], optimization-based approaches [6-9], learning-based approaches [10-12], and using the null space in a MIMO channel [13-16]. In particular, the PAPR reduction method using the null space can reduce PAPR of the MIMO-OFDM signals while avoiding MU interference, in-band distortion, and out-of-band radiation. Moreover, this method can utilize all transmission bandwidth and transmitter antennas for data transmission, unlike tone reservation [4] and antenna reservation [5]. From the above, although many PAPR reduction methods exist, we focus on and investigate the PAPR reduction method using the null space in a MIMO channel. Notice that the optimization-based methods in [7] and [8] also utilize the null space.

In [13], our research group originally reported PAPR reduction method using the null space in a MIMO channel. This method prevents PAPR reduction signals from degrading the throughput by transmitting them to only the null space in the MIMO channel. As a further advance, we also proposed the complexity-reduced PAPR reduction methods based on peak cancellation (PC) signals using the null space in the MIMO channel [14-16], which is referred to as PC with channel-null constraint (PCCNC). The original idea of PC signal-based method was reported in [17, 18]. In PCCNC, all the transmission signals for transmitter antennas are jointly considered as a vector form. The PC signal in the time domain is generated based on the sinc function, whose transmission bandwidth is equal to that of the OFDM signal, to avoid out-of-band radiation. Besides, the PC signal is restricted to the null space in the MIMO channel by the proper projection before transmission. Thus, by directly adding the PC signal vector to the data transmission signal after BF in the time domain, PAPR is reduced without in-band distortion and out-of-band radiation. Notice that MU interference is completely eliminated by applying zero forcing (ZF) based BF to the data stream.

However, PAPR reduction methods using the null space, such as PCCNC, suffer from high computational complexity, especially when the transmitter, such as base station (BS), is equipped with a large number of antennas, e.g., more than 100 antennas. Note that optimization-based approaches also have this fundamental challenge. This problem indicates that the calculation of the null space in the massive MIMO channel needs relatively high computational complexity. In addition, we emphasize that the iterative approaches, including PCCNC, have to cope with the increase in computational complexity due to the projection of the PC signal iteratively. Although using multiple transmitter antennas and iterations of processing can enhance the PAPR reduction capability, they make these PAPR reduction methods less feasible. Therefore, the objective of this paper is to realize a low-complexity PAPR reduction in a massive MIMO-OFDM system while keeping the sufficient PAPR reduction capability.

In this paper, we propose a new algorithm decreasing the dimension of the null space in the MIMO channel by dividing the transmitter antennas jointly considered in the PAPR reduction process to reduce computational complexity. Since the low-dimensional null space may degrade the PAPR reduction capability, the proposed algorithm executes the processing of PCCNC in parallel to realize efficient PAPR reduction. Through computer simulation, we demonstrate the superiority of the proposed algorithm and analyze the judicious balance of the trade-off between PAPR reduction capability and computational complexity.

979-8-3503-7099-7/24/$31.00 ©2024 IEEE

The remainder of the paper is organized as follows. First, Section II describes the process of PCCNC and reasons of increasing computational complexity. Section III describes the proposed parallel PCCNC scheme. Section IV shows the numerical results based on computer simulations. Finally, Section V concludes the paper.

II. Process of PCCNC and Reasons for Increasing Computational Complexity

We consider a downlink MU-MIMO system, where a BS transmitter equipped with N antennas serves M single antenna user terminals simultaneously. In this paper, we assume $N > M$. The block diagram of BS transmitter with PCCNC is illustrated in Fig. 1. First, the OFDM signals, where the number of fast Fourier transform (FFT)/inverse FFT (IFFT) points is F, is generated as the data stream. Subsequently, the data signal vector is generated by applying BF to the OFDM signals. The high PAPR of the OFDM signals may be further enhanced due to the BF process. Thus, we apply PCCNC in order to generate the low PAPR transmission signal vector. In PCCNC, the PAPR reduction process is only executed at the BS and process at each receiver (user terminal) side is unnecessary.

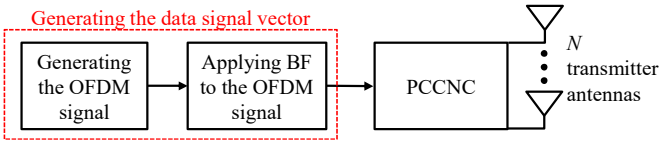

Fig. 1. Block diagram of BS transmitter with PCCNC.

For simplicity, we assume that the MIMO channel is not frequency selective. The $M \times N$-dimensional MIMO channel matrix is denoted as $\mathbf{H}$. The $N \times (N–M)$-dimensional matrix $\mathbf{V}$ corresponds to the null space in a MIMO channel, which satisfies $\mathbf{HV} = \mathbf{O}$. All the $N–M$ column vectors in $\mathbf{V}$ are orthonormalized each other. Let $\mathbf{B}$ and $\mathbf{s}[t]$ denote the $N \times M$-dimensional BF matrix and the M-dimensional data stream vector at discrete time t ($t = 1, ..., F$), respectively. Then, the N-dimensional time-domain data signal vector before PAPR reduction at time t denoted, $\mathbf{x}[t]$, can obtained by

$$\mathbf{x}[t] = [x_1[t] \quad \cdots \quad x_N[t]]^T = \mathbf{Bs}[t], \tag{1}$$

where $x_n[t]$ denotes the n-th element of $\mathbf{x}[t]$, which is transmitted from the n-th transmitter antenna.

In the following, we describe the detail of PCCNC with the block diagram shown in Fig. 2. PCCNC exploits the PC signal vector to reduce the PAPR of the transmission signal. Before its addition to the time-domain data signal vector $\mathbf{x}[t]$, the BF different from the one for the data stream is applied to the PC signal to suppress the signal power levels of all transmitter antennas and to restrict the signal to the null space in the MIMO channel (avoid the interference with the data streams). To realize these conditions, PCCNC is composed of the following two steps.

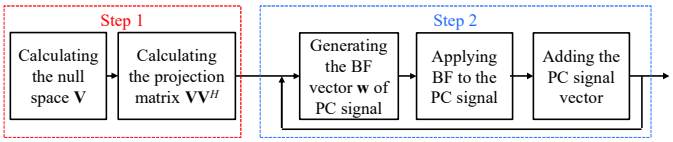

Fig. 2. Block diagram of PCCNC.

- Step 1: Introduction of the null space $\mathbf{V}$ and the projection matrix onto the null space $\mathbf{VV}^H$.
- Step 2: Adding the PC signal vector which is restricted to the null space in the MIMO channel.

The purpose of step 1 is calculation of the projection matrix in advance to be utilized for the null constraint. To achieve significant PAPR reduction, it is necessary that step 2 is performed many iterations.

The PC signal $g[t]$ is defined as the sinc function whose transmission bandwidth is equal to that of the OFDM signal and whose dominant peak amplitude at $t = 0$ is set to 1. To generate the PC signal vector $\mathbf{p}[t]$, we apply BF to $g[t]$ shifted to target timing. Specifically, we multiply BF vector of PC signal $\mathbf{w}$, which suppress the peak signals of transmission signal at a single target timing and projected onto the null space in the MIMO channel, to $g[t]$.

Let $\mathbf{x}^{(j)}[t] = [x_1^{(j)}[t] \quad \cdots \quad x_N^{(j)}[t]]^T$ denote the time-domain transmission signal vector at the j-th iteration of PCCNC. This vector is initialized to be the original data signal vector $\mathbf{x}[t]$, namely $\mathbf{x}^{(1)}[t] = \mathbf{x}[t]$. At the j-th iteration, PCCNC intends to reduce the PAPR observed in $\mathbf{x}^{(j)}[t]$ at the target time index, $\tau^{(j)}$. We decide the time index t, in which $x_n^{(j)}[t]$ has the maximum amplitude for all $n = 1, \ldots, N$ and $t = 0, \ldots, F–1$, as $\tau^{(j)}$. In the j-th iteration of PCCNC, the PC signal vector, $\mathbf{p}^{(j)}[t]$, which is given by (2), is added to $\mathbf{x}^{(j)}[t]$ to reduce the PAPR, like (3).

$$\mathbf{p}^{(j)}[t] = \mathbf{w}^{(j)} g[t - \tau^{(j)}]. \tag{2}$$

$$\mathbf{x}^{(j+1)}[t] = \mathbf{x}^{(j)}[t] + \mathbf{p}^{(j)}[t]. \tag{3}$$

The N-dimensional BF vector of PC signal, $\mathbf{w}^{(j)}$, suppresses the peak powers of transmission signal vector at a single target timing and is projected onto the null space in the MIMO channel. PC signal vector $\mathbf{p}^{(j)}[t]$ generated by multiplying $\mathbf{w}^{(j)}$ to the $\tau^{(j)}$-time-shifted version of $g[t]$, avoids out-of-band radiation and interference with the data streams. This is because the PC signal is transmitted through only the null space in the given MIMO channel and is not observed at the receiver side. In generating $\mathbf{w}^{(j)}$, the first step is to find the desirable BF vector of PC signal vector $\tilde{\mathbf{w}}^{(j)}$ from PAPR reduction perspective. After that, $\mathbf{w}^{(j)}$ is generated by the projection of $\tilde{\mathbf{w}}^{(j)}$ onto the null space $\mathbf{V}$ in the MIMO channel. In this paper, we design $\tilde{\mathbf{w}}^{(j)}$ and $\mathbf{w}^{(j)}$ based on [14], which can be expressed as follows:

$$\tilde{\mathbf{w}}^{(j)} = [\tilde{w}_1^{(j)} \quad \cdots \quad \tilde{w}_N^{(j)}]^T$$

$$\text{where } \tilde{w}_n^{(j)} = \begin{cases} \sqrt{P_{\text{th}}} e^{j\theta_n^{(j)}[\tau^{(j)}]} - x_n^{(j)}[\tau^{(j)}], & |x_n^{(j)}[\tau^{(j)}]|^2 > P_{\text{th}} \\ 0, & \text{Otherwise} \end{cases}. \tag{4}$$

$$\mathbf{w}^{(j)} = \mathbf{VV}^H \tilde{\mathbf{w}}^{(j)}. \tag{5}$$

Here, P_{th} is the power threshold, and $\theta_n^{(j)}[\tau^{(j)}]$ is the phase of $x_n^{(j)}[\tau^{(j)}]$. Note that $\tilde{\mathbf{w}}^{(j)}$ of (4) is the desirable PAPR reduction vector since the transmission power levels of all N transmitter antennas at time $\tau^{(j)}$, i.e., $|x_n^{(j)}[\tau^{(j)}]|^2$ for all n, can simultaneously be equal to or lower than P_{th} when $\tilde{\mathbf{w}}^{(j)}$ is directly used as $\mathbf{w}^{(j)}$ in (2) (without the projection of (5)).

When PCCNC is straightforwardly applied to a massive MIMO-OFDM system, which employs a large number of antennas, the system may suffer from a high computational complexity for PAPR reduction. We explain three reasons why PCCNC requires high computational complexity when a large number of antennas are used. Note that the number of real multiplications is used to evaluate the computational complexity in this paper.

- Step 1 consists of the calculations of the null space $\mathbf{V}$ and the projection matrix $\mathbf{V}\mathbf{V}^H$. However, the number of real multiplications of these calculations is proportional to the cube of the number of transmitter antennas.
- Step 2 includes the projection of $\tilde{\mathbf{w}}^{(j)}$ onto the null space in the MIMO channel in (5). Since this operation is required iteratively, the computational complexity is likely to be high to achieve a sufficient PAPR reduction capability.
- In [14], the PC signal for suppression of the peak power at a single timing is generated per iteration. This indicates that the number of timings to suppress peak power per iteration is limited to one. Therefore, the required number of iterations increases to achieve a sufficient PAPR reduction capability.

III. Proposed Parallel PCCNC Using Low-Dimensional Null Space

To reduce the computational complexity, we propose a parallel PCCNC using the low-dimensional null space. Specifically, the dimension of the null space is decreased by dividing the transmitter antennas jointly considered in PCCNC into antenna blocks. Moreover, due to independent parallel PCCNC for each antenna block, the peak powers at the timing for the number of antenna blocks are suppressed simultaneously per iteration. In the following, we describe the proposed parallel PCCNC.

The block diagram of the proposed parallel PCCNC is shown in Fig. 3. Let A denote the number of antenna blocks. A is assumed to be set to the value that makes the number of transmitter antennas per antenna block, N/A, satisfy $N/A > M$.

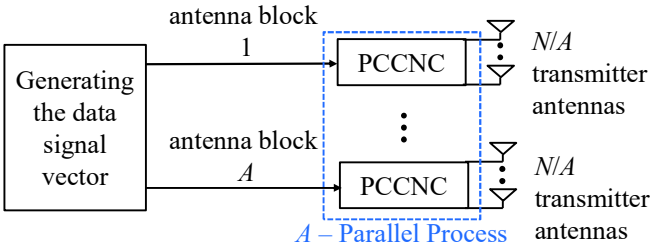

Fig. 3. Block diagram of the proposed parallel PCCNC.

Antenna block a is comprised of the $(a-1)(N/A)+1$-th to the $a(N/A)$-th transmitter antennas. Thus, at the j-th iteration, the PAPR reduction in antenna block a is applied to the (N/A)-dimension vector composed of the elements from the $(a-1)(N/A)+1$-th element to the $a(N/A)$-th element in $\mathbf{x}^{(j)}[t]$, which is given by

$$\mathbf{x}_a^{(j)}[t] = [x_{a,1}[t] \quad \cdots \quad x_{a,N/A}[t]]^T = [x_{(a-1)N/A+1}[t] \quad \cdots \quad x_{aN/A}[t]]^T . \quad (6)$$

The $M \times (N/A)$-dimensional MIMO channel matrix of antenna block a is denoted as $\mathbf{H}_a$. Since $N/A > M$, the $(N/A) \times (N/A-M)$-dimensional matrix $\mathbf{V}_a$ corresponds to the null space in the MIMO channel of antenna block a, which satisfies $\mathbf{H}_a\mathbf{V}_a = \mathbf{O}$. All the $(N/A-M)$ column vectors in $\mathbf{V}_a$ are orthonormalized each other.

In antenna block a, we decide the target time index $\tau_a^{(j)}$ based on $\mathbf{x}_a^{(j)}[t]$, where $x_{a,n}^{(j)}[t]$ for all $n = 1, \ldots, N/A$ and $t = 0, \ldots, F-1$ has the maximum amplitude at j-th iteration. By adding the PC signals in all the A antenna blocks respectively, PAPR is reduced in the proposed parallel PCCNC.

$$\mathbf{p}_a^{(j)}[t] = \mathbf{w}_a^{(j)} g[t - \tau_a^{(j)}] . \quad (7)$$

$$\mathbf{x}^{(j+1)}[t] = \begin{bmatrix} \mathbf{x}_1^{(j)}[t] \\ \vdots \\ \mathbf{x}_A^{(j)}[t] \end{bmatrix} + \begin{bmatrix} \mathbf{p}_1^{(j)}[t] \\ \vdots \\ \mathbf{p}_A^{(j)}[t] \end{bmatrix} . \quad (8)$$

$\mathbf{p}_a^{(j)}[t]$ is the (N/A)-dimensional PC signal vector in antenna block a. $\mathbf{w}_a^{(j)}[t]$ is the (N/A)-dimensional BF vector of PC signal vector in antenna block a, which is represented as

$$\tilde{\mathbf{w}}_a^{(j)} = [\tilde{w}_{a,1}^{(j)} \quad \cdots \quad \tilde{w}_{a,N/A}^{(j)}]^T$$
$$\text{where } \tilde{w}_{a,n}^{(j)} = \begin{cases} \sqrt{P_{\text{th}}} e^{j\theta_{a,n}^{(j)}[\tau_a^{(j)}]} - x_{a,n}^{(j)}[\tau_a^{(j)}], & |x_{a,n}^{(j)}[\tau_a^{(j)}]|^2 > P_{\text{th}} \\ 0, & \text{Otherwise} \end{cases} . \quad (9)$$

Here, $\theta_{a,n}^{(j)}[\tau_a^{(j)}]$ is the phase of $x_{a,n}^{(j)}[\tau_a^{(j)}]$. $\tilde{\mathbf{w}}_a^{(j)}$ is the desirable PAPR reduction vector as in (4). Finally, to generate $\mathbf{w}_a^{(j)}[t]$, $\tilde{\mathbf{w}}_a^{(j)}$ is projected onto the null space in the MIMO channel of antenna block a by

$$\mathbf{w}_a^{(j)} = \mathbf{V}_a \mathbf{V}_a^H \tilde{\mathbf{w}}_a^{(j)} . \quad (10)$$

Since the proposed parallel PCCNC decreases the number of transmitter antennas jointly considered for PAPR reduction by $1/A$, the number of real multiplications is significantly reduced for step 1 and step 2, respectively. In addition, since one iteration of the proposed parallel PCCNC can suppress peak powers at different timings, the required number of iterations for a sufficient PAPR reduction is reduced.

IV. Numerical Results

The relationship between the PAPR reduction capability and computational complexity of PCCNC is evaluated based on computer simulations. Note that the proposed parallel PCCNC for $A = 1$ corresponds to the conventional PCCNC in Section II. We assume that the BS has $N = 100$ transmitter antennas and serves $M = 4$ single-antenna users. In addition, we assume MU MIMO-OFDM transmission with applying ZF-based BF to the data stream. We consider the OFDM signal with 64 subcarriers. The number of FFT/IFFT points, F, is set to 256, which corresponds to 4-times oversampling in the time domain to measure the PAPR levels accurately [19]. We used 64-ary quadrature amplitude modulation (64-QAM) with Gray mapping for data modulation. The channel model is assumed to be flat Rayleigh fading, in which each element of $\mathbf{H}$ follows the i.i.d. standard complex Gaussian distribution. Power threshold P_{th} is defined as the signal power threshold normalized by the signal power per antenna averaged over the channel realizations. In this papar, P_{th} is set to 4 dB. In all simulations, we normalize the transmission signal power after PAPR reduction to one. We define the PAPR of transmission signal at j-th iteration $\mathbf{x}^{(j)}$ as the ratio of the highest peak power to its average power over all transmitter antennas and one OFDM symbol duration, which is given by

$$PAPR = \frac{\max_{0 \le t \le F-1, 1 \le n \le N} \left[\left| x_n^{(j)}[t] \right|^2 \right]}{\sum_{t=0}^{F-1} \left\| \mathbf{x}^{(j)}[t] \right\|_2^2 / NF} . \quad (11)$$

To measure the influence of decreasing the dimension of the null space on the transmission quality, we define the ratio of the

total PC signal power up to j-th iteration to the transmission signal power, as follows

$$R_{\mathrm{PC}} = \frac{\sum_{t=0}^{F-1}\left\|\sum_{j=1}^{J}\mathbf{p}^{(j)}[t]\right\|_2^2}{\sum_{t=0}^{F-1}\left\|\mathbf{x}^{(j)}[t]\right\|_2^2}. \tag{12}$$

Figs. 4 and 5 show the average R_{PC} as a function of J and the average bit-error-rate (BER) as a function of the signal-to-noise ratio (SNR) when J = 1000, respectively. The SNR at j-th iteration is defined as

$$SNR = \frac{\sum_{t=0}^{F-1}\left\|\mathbf{x}^{(j)}[t]\right\|_2^2 / NF}{N_0}. \tag{13}$$

In Figs. 4 and 5, the red, green, blue and orange lines show cases of the proposed PCCNC with A = 2, 4, 5 and 10, respectively. In Fig. 5, the BER performance of no PAPR reduction is represented as an ideal case. The dotted black line shows a case of the PCCNC with A = 1, which corresponds to the conventional PCCNC. From Fig. 4, the average R_{PC} of the proposed PCCNC is larger than that of the conventional PCCNC. This is because the power loss to cancel the elements that interfere with the data stream by projecting the PC signals onto the null space becomes larger due to decreasing the proportion of streams corresponding to the null space among all streams as A increases. From Fig. 5, the BER performance decreases as A increases. It is worth noting that BER performances for A = 2, 4 and 5 are slightly degraded compared with the conventional PCCNC. This is because in the proposed PCCNC when A = 2, 4 and 5, in-band distortion due to the PC signal can be eliminated by transmitted to only the null space with low transmission power loss. This suggests that the proposed parallel PCCNC with A = 2, 4 and 5 have the sufficient dimension of the null space for the PAPR reduction.

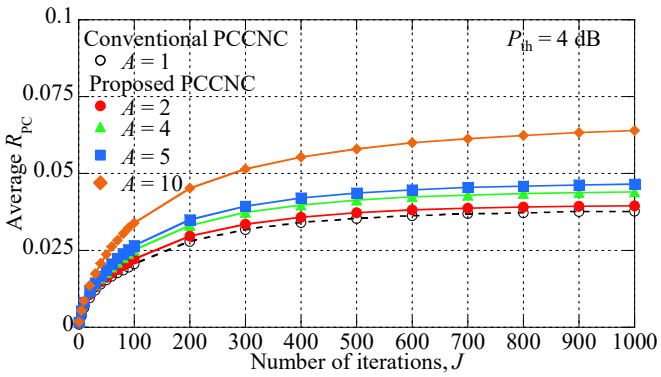

Fig. 4. The average R_{PC} as a function of J.

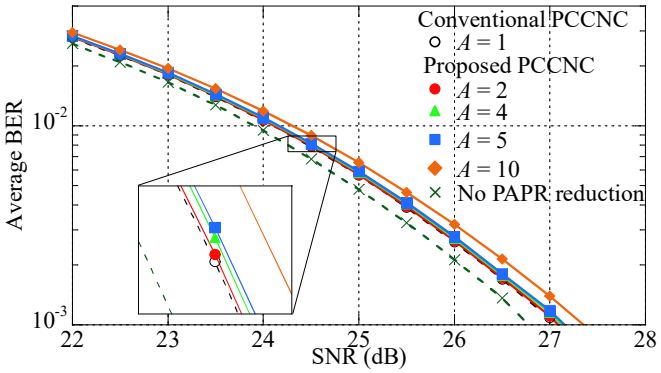

Fig. 5. The average BER as a function of the SNR.

Fig. 6 shows the complementary cumulative distribution function (CCDF) of the PAPR when J = 100 and 1000. From Fig. 6, when many iterations are acceptable, the PAPR is sufficiently reduced for P_{th} regardless of A. This indicates the dimension of the null space is sufficient for the PAPR reduction for each antenna block. On the other hand, when the number of iterations is small, the proposed parallel PCCNC achieves a lower PAPR than the conventional PCCNC. This is because the peak powers which should be suppressed preferentially are suppressed with fewer iterations due to the parallel PCCNC for each antenna block. Thus, the efficient PAPR reduction is achieved by the proposed PCCNC.

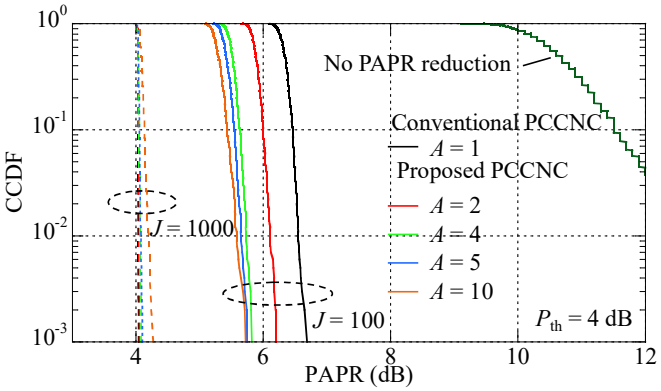

Fig. 6. The CCDF of the PAPR.

To analyze the convergence rate of the proposed parallel PCCNC, Fig. 7 shows the average PAPR as function of J. From Fig. 7, the PAPR converges with the fewer number of iterations when the proposed parallel PCCNC is applied to the system. This confirms the validity of conclusion regarding Fig. 6. Therefore, the proposed parallel PCCNC has the potential to realize the efficient PAPR reduction capability.

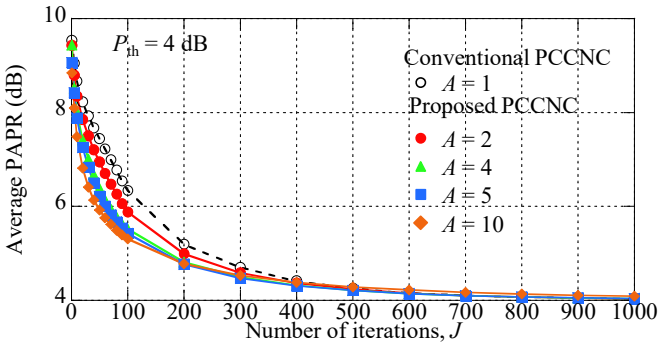

Fig. 7. The average PAPR as a function of J.

Since the computational complexity varies depending on A, we compare the PAPR-vs.-the number of real multiplications performance with different A. TABLE I shows the number of real multiplications with J iterations. The number of real multiplications is a function of N, M, J, F and A.

TABLE I. NUMBER OF REAL MULTIPLICATIONS

PAPR reduction method	Process		Number of real multiplications
PCCNC	Step 1	Calculating the null space $\mathbf{V}_a$	$4A\,(N/A)^3+2A\,(N/A)^2$
		Calculating the projection matrix $\mathbf{V}_a\mathbf{V}_a^H$	$4A\,(N/A)^2(N/A-M)$
	Step 2	Generating the BF vector of PC signal	$J(4A\,(N/A)^2+4N)$
		Applying BF to the PC signal	JNF

Finally, Fig. 8 shows the average PAPR as a function of the number of real multiplications for PCCNC. The relationship between the number of real multiplications and the average PAPR is evaluated by varying the J value for respective A. The proposed parallel PCCNC achieves significant reduction the number of real multiplications for the same PAPR compared to the conventional PCCNC. This is because, in the proposed parallel PCCNC, the benefits of the computational complexity reduction and the efficiency of parallel PCCNC can be obtained.

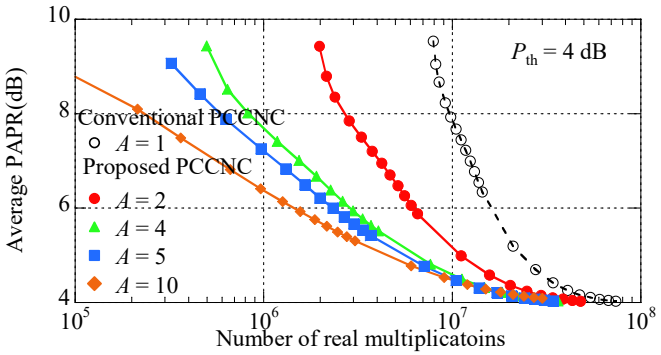

Fig. 8. The average PAPR as a function of the number of real multiplications for PCCNC.

V. CONCLUSION

In this paper, we proposed a parallel PCCNC using the low-dimensional null space. The proposed PCCNC divides the transmitter antennas jointly considered in the PAPR reduction process, to reduce the computational complexity. In addition, an efficient PAPR reduction is achieved due to the processing in parallel. Numerical results showed that the proposed PCCNC can balance the computational complexity and the PAPR reduction capability. The extension of the proposed PCCNC is to accommodate the frequency selective channel to utilize the approach in [15].

REFERENCES

[1] Z. Zhang, et al., "6G wireless networks: Vision, requirements, architecture, and key technologies," IEEE Veh. Technol. Mag., vol. 14, no. 3, pp. 28-41, Sep. 2019.
[2] T. L. Marzetta, "Noncooperative cellular wireless with unlimited numbers of base station antennas," IEEE Trans. On Wireless Commun., vol. 9, no. 11, pp. 3590-3600, Nov. 2010.
[3] H. Papadopoulos, C. Wang, O. Bursalioglu, X. Hou, and Y. Kishiyama, "Massive MIMO technologies and challenges towards 5G," IEICE Trans. Commun., vol. E99-B, no. 3, pp. 602-621, Mar. 2016.
[4] C. Ni, Y. Ma, and T. Jiang, "A novel adaptive tone reservation scheme for PAPR reduction in large-scale multi-user MIMO-OFDM systems," IEEE Wireless Commun. Lett., vol. 5, no. 5, pp. 480-483, Oct. 2016.
[5] H. Prabhu, O. Edfors, J. Rodrigues, L. Liu, and F. Rusek, "A low-complex peak-to-average power reduction scheme for OFDM based massive MIMO systems," in Proc. ISCCSP2014, Athens, Greece, May 2014.
[6] C. Studer and E. G. Larsson, "PAR-aware large-scale multi-user MIMO-OFDM downlink," IEEE J. Sel. Areas Commun. vol. 31, no. 2, pp. 303-313, Feb. 2013.
[7] H. Bao, J. Fang, Q. Wan, Z. Chen, and T. Jiang, "An ADMM approach for PAPR reduction for large-scale MIMO-OFDM systems," IEEE Trans. Veh. Technol., vol. 67, no. 8, pp. 7407-7418, Aug. 2018.
[8] R. Zayani, H. Shaiek, and D. Roviras, "PAPR-aware massive MIMO-OFDM downlink," IEEE Access, vol. 7, pp. 25474-25484, Feb. 2019.
[9] S. Taner and C. Studer, "Alternating projections method for joint precoding and peak-to-average-power ratio reduction," in Proc. IEEE WCNC2023, Glasgow, Scotland, Mar. 2023.
[10] M. Kim, W. Lee, and D.-H. Cho, "A novel PAPR reduction scheme for OFDM system based on deep learning," IEEE Commun. Lett., vol. 22, no. 3, pp. 510-513, Mar. 2018.
[11] R. Kuwahara and M. Ohta, "PAPR and OOBE suppression of OFDM signal using deep learning," in Proc. IEEE GCCE2020, Kobe, Japan, Oct. 2020.
[12] A. Kalinov, R. Bychkov, A. Ivanov, A. Osinsky, and D. Yarotsky, "Machine learning-assisted PAPR reduction in massive MIMO," IEEE Wireless Commun. Lett., vol. 10, no. 3, pp. 537–541, Mar. 2021.
[13] R. Kimura, Y. Tajika, and K. Higuchi, "CF-based adaptive PAPR reduction method for block diagonalization-based multiuser MIMO-OFDM signals," in Proc. IEEE VTC2011-Spring, Budapest, Hungary, 15-18, May 2011.
[14] T. Suzuki, M. Suzuki, Y. Kishiyama, and K. Higuchi, "Complexity-reduced adaptive PAPR reduction method using null space in MIMO channel for MIMO-OFDM signals," IEICE Trans. Commun., vol. E103-B, no. 9, pp. 1019-1029, Sept. 2020.
[15] L. Yamaguchi, N. Nonaka, and K. Higuchi, "PC-signal-based PAPR reduction using null space in MIMO channel for MIMO-OFDM signals under frequency-selective fading channel," in Proc. IEEE VTC2020-Fall, Virtual conference, Nov.-Dec. 2020.
[16] J. Saito, N. Nonaka, K. Higuchi, "PAPR reduction using null space in MIMO channel considering power difference among transmitter antennas," in Proc. IEEE WCNC2023, Glasgow, Scotland, Mar. 2023.
[17] T. Hino and O. Muta, "Adaptive peak power cancellation scheme under requirements of ACLR and EVM for MIMO-OFDM systems," in Proc. IEEE PIMRC2012, Sydney, Australia, Sept. 2012.
[18] T. Kageyama, O. Muta, and H. Gacanin, "An adaptive peak cancellation method for linear-precoded MIMO-OFDM signals," in Proc. IEEE PIMRC2015, Hong Kong, 30 Aug.-2 Sept. 2015.
[19] M. Sharif, M. Gharavi-Alkhansari, and B. H. Khalaj, "On the peak-to-average power of OFDM signals based on oversampling," IEEE Trans. Commun., vol. 51, no. 1, pp. 72-78, Jan. 2003.